GEOLOGY

Volcanic mercury and mutagenesis in land plants during the end-Triassic mass extinction

Sofie Lindström[1]*, Hamed Sanei[2], Bas van de Schootbrugge[3], Gunver K. Pedersen[1], Charles E. Lesher[2,4], Christian Tegner[2], Carmen Heunisch[5], Karen Dybkjær[1], Peter M. Outridge[6]

During the past 600 million years of Earth history, four of five major extinction events were synchronous with volcanism in large igneous provinces. Despite improved temporal frameworks for these events, the mechanisms causing extinctions remain unclear. Volcanic emissions of greenhouse gases, SO_2, and halocarbons are generally considered as major factors in the biotic crises, resulting in global warming, acid deposition, and ozone layer depletion. Here, we show that pulsed elevated concentrations of mercury in marine and terrestrial sediments across the Triassic-Jurassic boundary in southern Scandinavia and northern Germany correlate with intense volcanic activity in the Central Atlantic Magmatic Province. The increased levels of mercury—the most genotoxic element on Earth—also correlate with high occurrences of abnormal fern spores, indicating severe environmental stress and genetic disturbance in the parent plants. We conclude that this offers compelling evidence that emissions of toxic volcanogenic substances contributed to the end-Triassic biotic crisis.

INTRODUCTION

The end-Triassic mass extinction at 201.51 million years (Ma) (*1*, *2*) is considered to be one of the most severe biotic crises during the Phanerozoic, with substantial impact on both marine and terrestrial ecosystems (*3*). This extinction is generally explained by global warming due to massive input of CO_2 and/or methane to the atmosphere from volcanic activity in the Central Atlantic Magmatic Province (CAMP) (*4*, *5*), the most extensive large igneous province (LIP) on Earth (*6*). High-precision radioisotope ages of CAMP volcanic rocks show that magmatic activity commenced c. 100,000 years before the end-Triassic event (*7*) and continued in pulses for 700,000 years (Fig. 1A) (*8*). As shown by major perturbations in $\delta^{13}C$ records across the Triassic-Jurassic boundary (TJB), prolonged and voluminous volcanism released vast quantities of the greenhouse gas CO_2, as well as SO_2, and other potentially toxic compounds to the atmosphere (*4*–*6*, *9*). The presence of altered volcanic glass spherules, euhedral pyroxene, and amphibole pseudomorphs (*10*) and increased levels of iridium in marine sediments (*11*) are indicative of the far reach of CAMP activity, but ash beds from CAMP are thus far lacking outside the CAMP area. In preindustrial sedimentary records, temporal distribution of mercury (Hg) is considered a suitable proxy for fallout from volcanic activity (*12*–*13*). Mercury is emitted primarily as gaseous Hg not only via explosive volcanism but also via degassing from nonexplosive volcanism (*14*). Distribution of gaseous Hg (and other substances) from CAMP would have been governed by atmospheric circulation and high-altitude wind patterns (*15*). The long residence time in the atmosphere of gaseous elemental Hg (Hg^0), from 6 months to 2 years, would promote global or at least hemispheric distribution of this element (*15*). Elevated Hg concentrations in sedimentary rocks (i.e., Hg anomaly) in marine TJB successions of Nevada (*16*), Canada, Greenland, England, Austria, Morocco, and Peru (*17*) have been linked to CAMP eruptions, suggesting widespread reach of volcanic Hg from the CAMP. Recently, the use of Hg in sedimentary successions as a proxy for LIP volcanic activity has been questioned (*18*, *19*), as Hg can also be distributed to sedimentary basins by other sources. However, the possibly global and contemporaneous increase in Hg in both terrestrial and marine TJB successions (*16*, *17*, *20*) suggests increased input of Hg to the global mercury cycle at that time. Thus, the distribution of volcanic Hg in the TJB sedimentary record could potentially provide a means to probe the relationship between CAMP volcanic pulses and biotic responses at various sites.

Here, we focus on investigating the possible correlation of Hg loading with evidence of stress responses of terrestrial plants in the fossil record, specifically in the palynological record. We know today that, apart from greenhouse and other gases, volcanic activity can emit a range of known primary phytotoxic pollutants, including Hg and other heavy metals, fluoride, O_3, SO_2, and polycyclic aromatic hydrocarbons (PAHs) (*21*). Phytotoxic substances can induce stress responses and cause morphologically visible abnormalities not only in the parent plants (e.g., stunted growth, lesions, necrosis, and shortening of roots) but also in the reproductive cells, i.e., spores and pollen (*22*). Studies of both extant and fossil plants suggest that normal sporogenesis results in 95 to 97% viable spores and 3 to 5% aberrant, nonviable spores (*23*–*26*). Therefore, aberrant spore quantities above 5% are generally regarded as indications of environmental stress. Because of the durability of their sporopollenin walls, abnormal pollen and spores can be used as bioindicators of environmental stress in preindustrial sediments—an especially useful proxy for phytotoxicity in the fossil record. However, it is necessary to differentiate between nonmutagenic and mutagenic aberrant spores or pollen, where the former can be induced through various environmental stresses (e.g., drought, frost, and water logging) disrupting the spore or pollen maturation process, commonly resulting in premature shedding of immature spores or pollen that may or may not be retained and dispersed in tetrads. Mutagenic changes in the mother plant, on the other hand, lead to an increase in the number of spores or pollen that are aberrant and nonviable. A few studies have noted increased abundances of aberrant spores and pollen during other extinction events linked to LIPs and have mainly attributed these

[1]Geological Survey of Denmark and Greenland, Øster Voldgade 10, DK-1350 Copenhagen K, Denmark. [2]Department of Geoscience, Aarhus University, Hoegh-Guldbergs Gade 2, DK-8000 Aarhus C, Denmark. [3]Department of Earth Sciences, Marine Palynology and Paleoceanography, Utrecht University, Princetonlaan 8A, 3584 CB Utrecht, Netherlands. [4]Department of Earth and Planetary Sciences, University of California, Davis, Davis, CA 95616, USA. [5]State Authority for Mining, Energy and Geology, Stilleweg 2, D-30655 Hannover, Germany. [6]Geological Survey of Canada, Natural Resources Canada, 601 Booth Street, Ottawa, Ontario K1A 0E8, Canada.
*Corresponding author. Email: sli@geus.dk

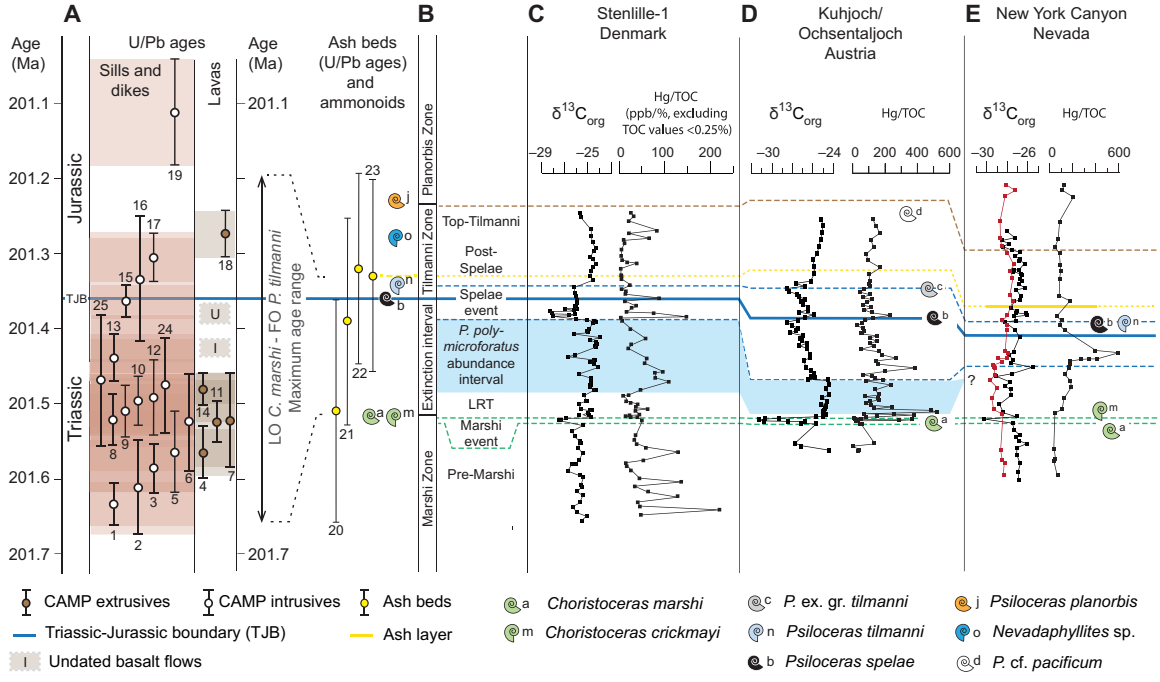

Fig. 1. TJB timeline and correlation of the Stenlille-1 record with Kuhjoch, Austria, and New York Canyon, Nevada. (**A**) U/Pb ages for CAMP intrusives (white circles), CAMP basalts (brown circles), and ash beds from Nevada and Peru (yellow circles), and ammonoid events (*1*, *7*, *8*, *32*, *34*). Note that U/Pb ages 4, 7, 11, and 14 are all from the North Mountain Basalt. 1, Kakoulima intrusion (*7*); 2, Tarabuco sill (*7*); 3, Messejana dike (*7*); 4, North Mountain Basalt (*8*); 5, Amelal sill (*8*); 6, Amazonas sill (low Ti) (*7*); 7, North Mountain Basalt (*7*, *8*); 8, Palisades sill (*8*), feeder of the Orange Mountain Basalt; 9, York Haven intrusive (*8*); 10, Rapidan intrusive (*8*); 11, North Mountain Basalt (*7*); 12, Fouta Djalon sill (*7*); 13, Hodh sill (*7*); 14, North Mountain Basalt (*1*, *2*); 15, Amazonas sill (high Ti) (*7*); 16, Shelburne dike (*7*); 17, Rossville intrusive (*8*); 18, Preakness Basalt (*8*); 19, Foum Zguid (*7*); 20, Ash bed LM4-86, Peru (*1*, *2*); 21, Ash bed LM4-90, Peru (*1*, *2*); 22, Ash bed NYC-N10, Nevada (*1*); 23, Ash bed LM4-100/101, Peru (*1*, *2*); 24, Amazonas Basin sill, Brazil (*33*); 25, Solimões Basin sill, Brazil (*33*). (**B**) Ammonite zones and extinction interval (*32*). (**C** to **E**) Bulk organic C-isotope (as ‰ of Vienna Pee Dee belemnite) (*9*, *32*) and Hg/TOC (in ppb/%) records for (C) Stenlille-1, (D) Kuhjoch, Austria (*17*, *34*), and (E) New York Canyon, Nevada (*16*). For an expanded version of this figure showing correlations of Hg/TOC-records and Hg -records of all studied localities, see fig. S2.

to mutagenic effects of a thinned ozone layer (*24*, *27*–*28*). Recent work demonstrates that elevated ultraviolet-B (UV-B) radiation increases malformations in pine pollen and that the resulting teratology (i.e., patterns of abnormal development) exhibits the same traits as those registered in gymnospermous bisaccate pollen during the end-Permian event (*29*), the most severe mass extinction of the last 540 Ma (*3*). Others have focused on the abundance of all abnormal spores and pollen across the Permian-Triassic boundary, suggesting that volcanic pollution from the Siberian Traps was responsible for the mutagenesis (*30*).

Here, we quantify various types of abnormalities in the reproductive cells of ferns, i.e., teratology of fossil fern spores, and use this as a proxy for ecological stress and possible mutagenesis in land plants across the TJB. We examined the teratology of two morphogroups of smooth-walled (laevigate), trilete fern spores with fairly thick exine, which we refer to as LTT-spores (laevigate, triangular, trilete spores) (Fig. 2, A to F) and LCT-spores (laevigate, circular, trilete spores) (fig. S1), in the Danish and North German basins. Several other spore and pollen taxa also exhibit abnormalities during the TJB interval (*31*); however, LTT- and LCT-spores are ideal to use as proxies for environmental-induced teratology as they are simple trilete spores with rather thick and unsculptured walls (exines). The exine thickness limits folding and, thus, enables distinction between malformed specimens and spores that are merely poorly preserved or folded. Similarly, the lack of complex ornamentation makes it easier to assess morphological abnormalities. Normal LTT-spores are triangular in outline, with a trilete mark with or without labra (Fig. 2, A to F), while normal spores of the LCT morphogroup are circular, commonly without, or with only thin labra (fig. S1, A to D). The two morphogroups exhibit similar aberrant forms that are ranked in categories as mild to severe teratology [severity categories (C) to (J) in Table 1], suggesting disturbance during different developmental stages (Table 1).

To correlate the teratology record with the CAMP volcanism, we compare the teratology to Hg loading in stratigraphically well-constrained (*32*) marine successions in cored wells from the Danish Basin (Stenlille-1 and Stenlille-4) and the North German Basin (Rødby-1), that span the TJB. We also present teratology and Hg data from outcrop and core samples from the predominantly terrestrial Rhaetian (latest Triassic) Norra Albert/Albert-1 succession in the Danish Basin to test contemporaneous Hg accumulation in the Rhaetian mires and freshwater systems.

RESULTS

The stratigraphic framework for this paper is based on correlations between radioisotopic (U/Pb) ages of ash beds in ammonite-bearing successions in Nevada and Peru (*1*, *2*), U/Pb ages of CAMP extrusives and intrusives (*7*, *8*, *33*), and ammonite and palynological events in sedimentary successions in Northwestern (NW) Europe (Fig. 1 and fig. S2) (*32*). This correlation allows recognition of three negative organic C-isotope excursions (CIEs): the Marshi, the Spelae, and the top-Tilmanni CIEs (Fig. 1). The interval below the Marshi

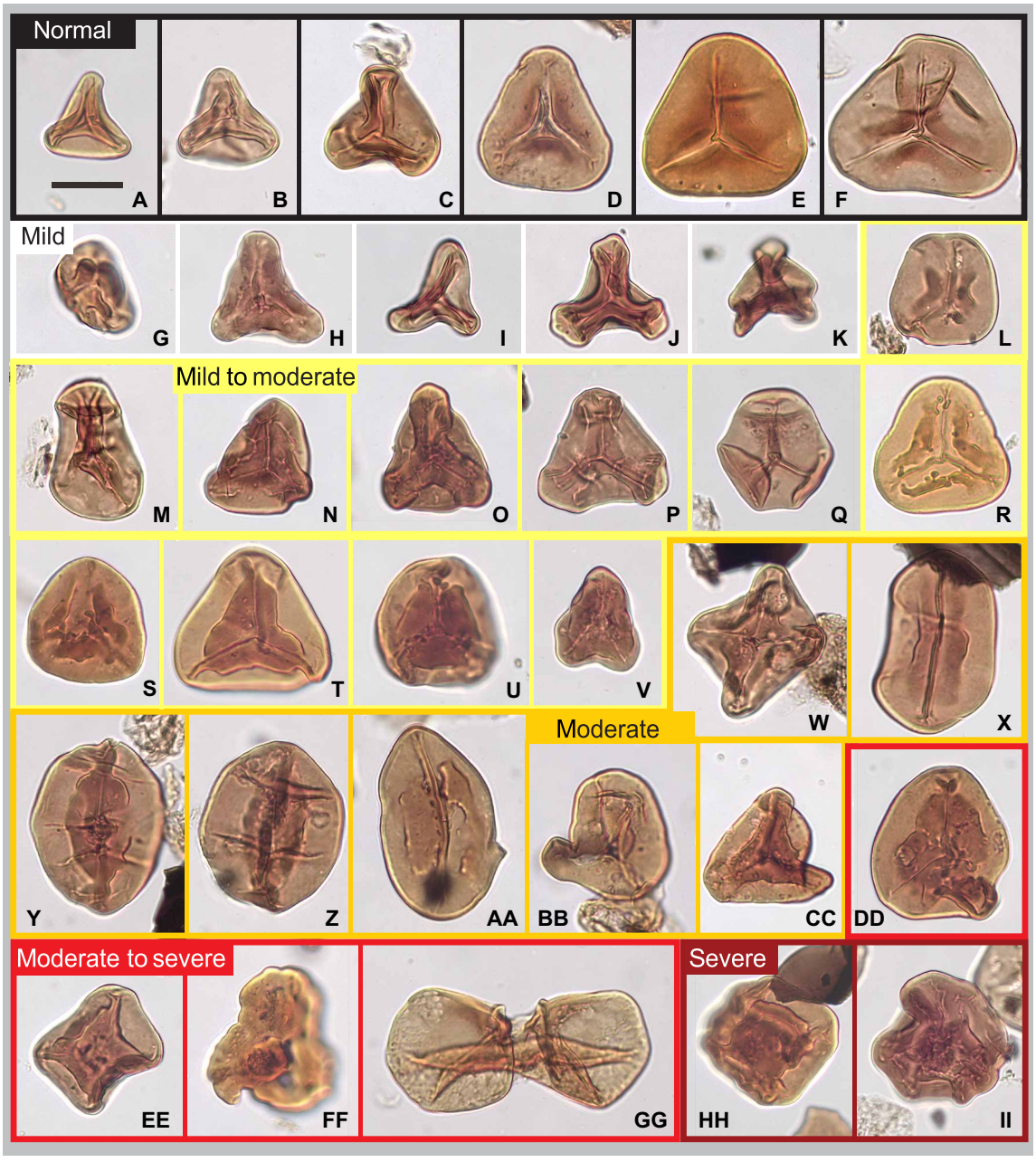

Fig. 2. Selected photos of LTT-spores teratology, arranged after teratology category defined in Table 1. In black frames: (**A** to **F**) representatives of normal spores. In white frames, mild teratology: (**G** and **H**) dwarfs, (**I** to **K**) unexpanded forms. In yellow frames, mild to moderate teratology: (**L** and **M**) uneven trilete mark, (**N**) uneven trilete mark and aberrant exine cracks, (**O** to **Q**) aberrant exine cracks or folds, (**R** to **U**) thickened labra or with growths, and (**V**) dwarf with thickened labra. In orange frames, moderate teratology: (**W**) quadrilete specimen, (**X**) monolete specimens with thickened labra, (**Y** and **Z**) mono- or multilete specimens, (**AA**) monolete specimen with deformed labra and possibly deformed outline, and (**BB** and **CC**) specimens with deformed outline. In light red frames, moderate to severe teratology: (**DD**) specimen with weakly deformed trilete mark and deformed outline, (**EE**) weakly deformed proximal area on a quadrilete specimen, (**FF**) weakly deformed proximal area with weakly discernable laesura and deformed outline, and (**GG**) conjoined twins. In dark red frames, severe teratology: (**HH** and **II**) severe proximal deformation. Scale bar, 20 μm. For sample number and England Finder coordinates, see table S1.

CIE is here referred to as the pre-Marshi interval. The Marshi CIE is expressed as a negative CIE close to the last occurrence of the typical Triassic ammonoid *Choristoceras marshi* or the closely related *Choristoceras crickmayi*. The Marshi event marks the onset of the end-Triassic mass extinction in marine successions (*32*, *34*). The Marshi CIE is in expanded successions succeeded by a maximum flooding event (*32*, *35*), herein referred to as the late Rhaetian transgression (LRT). In NW Europe, the LRT is followed by the *Polypodiisporites polymicroforatus* abundance interval, which can be recognized over large areas in both terrestrial and marine successions, and is characterized by generally high abundances of the nominate fern spore species (*32*). The *P. polymicroforatus* abundance interval is associated with a regressive event and more positive organic $\delta^{13}C$ values. The *P. polymicroforatus* abundance interval encompasses the maximum

Table 1. Teratology: Characterization, severity, and possible cause.

Teratology	Characteristics	Severity	Possible cause
(A) *Dwarfed forms*	Aberrant small size. Often dense exine. Immature.	Minor	Premature shedding.
(B) *Unexpanded forms*	Poorly inflated. Immature.	Minor	Premature shedding.
(C) *Uneven trilete rays*	Uneven length of trilete rays or deformed (sinuous) trilete rays.	Minor to moderate	One or more aborted spore in tetrad.
(D) *Aberrant folding*	Exine with transverse folds and/or cracks.	Minor to moderate	Mild genetic disturbance?
(E) *Labra thickened or with growths*	Aberrant wide labras or with growths (baculae, granae, and verrucae) on labra.	Minor to moderate	Mild genetic disturbance.
(F) *Mono- or multilete*	Aberrant mark with too few or too many rays.	Moderate	Disturbed meiosis resulting in either a tetragonal tetrad configuration, or more than 4 spores, or due to fused twins. Unbalanced cytokinesis.
(G) *Deformed outline*	Indentations on spore margin, not caused by folding or preservation.	Moderate	Probably not only related to uneven spore development in a tetrad. Genetic disturbance affecting cell growth. Incomplete cytokinesis.
(H) *Minor proximal deformation*	Thickened and/or wrinkled proximal area with trilete mark partially discernable.	Moderate to severe	Genetic deformation affecting the proximal (germination) area.
(I) *Deformed or fused tetrads or dyads*	Not merely separate spores still in tetrad or dyad configuration.	Moderate to severe	May indicate genetic disturbance and unbalanced cytokinesis.
(J) *Major proximal deformation*	Thickened and wrinkled proximal area where the trilete mark is not discernable.	Severe	Severe genetic deformation of proximal (germination) area.

phase of the marine extinction interval, and palynological data across Europe indicate widespread deforestation and major restructuring of the terrestrial ecosystem during this interval (*36*, *37*). The next CIE, the Spelae CIE, occurs before the first occurrence of the marker taxon for the basal Jurassic, the ammonite *Psiloceras spelae tirolicum* (*34*). The Spelae CIE is associated with a transgressive event and is generally marked by an initial sharp negative peak, followed by a plateau of somewhat less negative values (*4*, *32*). The Spelae CIE is characterized by depauperate benthic marine faunas, while plant communities appear to have begun to recover already around this event, albeit with spore-producing plants playing a more dominant role globally (*9*, *37*, *38*). The interval between the Marshi and Spelae CIEs corresponds roughly to the marine extinction interval (Fig. 1 and fig. S2). On the basis of correlations between U/Pb-dated ash beds in Peru and Nevada, the maximum age range for this interval is ~450 thousand years (ka), encompassing the hitherto dated CAMP extrusives, the North Mountain and the Preakness basalts (*1*, *7*, *8*) (Fig. 1 and fig. S2). Between these two dated CAMP extrusives, there are at least two additional basalt flows in Morocco (the Intermediate and the Upper units) that are not dated (*6*). Palynofloras from sediments above the Upper Unit in Morocco also indicate a Rhaetian age (*39*). The interval succeeding the Spelae CIE is characterized by positive C-isotope values and is referred to as the post-Spelae interval (Fig. 1). At the top of the Tilmanni ammonite zone, the organic $\delta^{13}C$ again shifts toward more negative values, and this shift is referred to as the top-Tilmanni CIE (*32*). This level equates to the onset of the "main CIE" of reference (*4*).

In the Stenlille wells (Danish Basin), we observe four distinct peaks where Hg increases by a factor of 10 or more above background levels [~12 to 15 parts per billion (ppb)] to maximum concentrations of 120 to 230 ppb (Figs. 3 and 4). Increased Hg levels are registered in the lower part of the pre-Marshi interval, during the LRT, the Spelae CIE, and just before the top-Tilmanni CIE (Figs. 3 and 4). In Rødby-1 (North German Basin), multiple Hg anomalies are evident with peak values up to 600 ppb, i.e., three to six times the background level at ~104 ppb, including during the LRT, the Spelae CIE, and just before the top-Tilmanni CIE (Fig. 3). In addition, the Rødby-1 record indicates elevated Hg levels above the top-Tilmanni CIE (Fig. 3). When Hg is normalized by total organic carbon (TOC) to account for Hg sequestration by organic matter, the pattern changes somewhat. Although Hg/TOC levels only appear to be elevated in the pre-Marshi interval of Stenlille-1 (Fig. 3), the two Stenlille wells otherwise show remarkably similar patterns during the LRT, *P. polymicroforatus* abundance interval, the Spelae CIE, and close to the top-Tilmanni CIE (Figs. 3 and 4). During the first part of the LRT, Hg input was elevated, but the overall Hg/TOC remained low (Figs. 3 and 4). In the upper part of the LRT, Hg and Hg/TOC levels both decrease despite high TOC levels (1 to 3%). During the *P. polymicroforatus* abundance interval, TOC values are low, but increased Hg/TOC levels are present in all three cores (Figs. 3 and 4). Likewise, elevated Hg during the Spelae CIE is marked by two Hg/TOC peaks in all three cores. During the post-Spelae interval, slight increases in both Hg and Hg/TOC are recorded just below the top-Tilmanni CIE in the Stenlille-1 and Rødby-1 records. In addition, both Hg and Hg/TOC values are elevated at a higher stratigraphic level in Rødby-1 (Fig. 3).

Malformations in LTT-spores, indicative of mutagenesis in the parent plants [severity categories (C) to (J), Table 1], first occur sporadically in the lower pre-Marshi interval (Fig. 3). In Stenlille-1 and Stenlille-4, up to 20% of the LTT-spores at this level are malformed, occasionally exhibiting moderate and moderate to severe mutagenesis

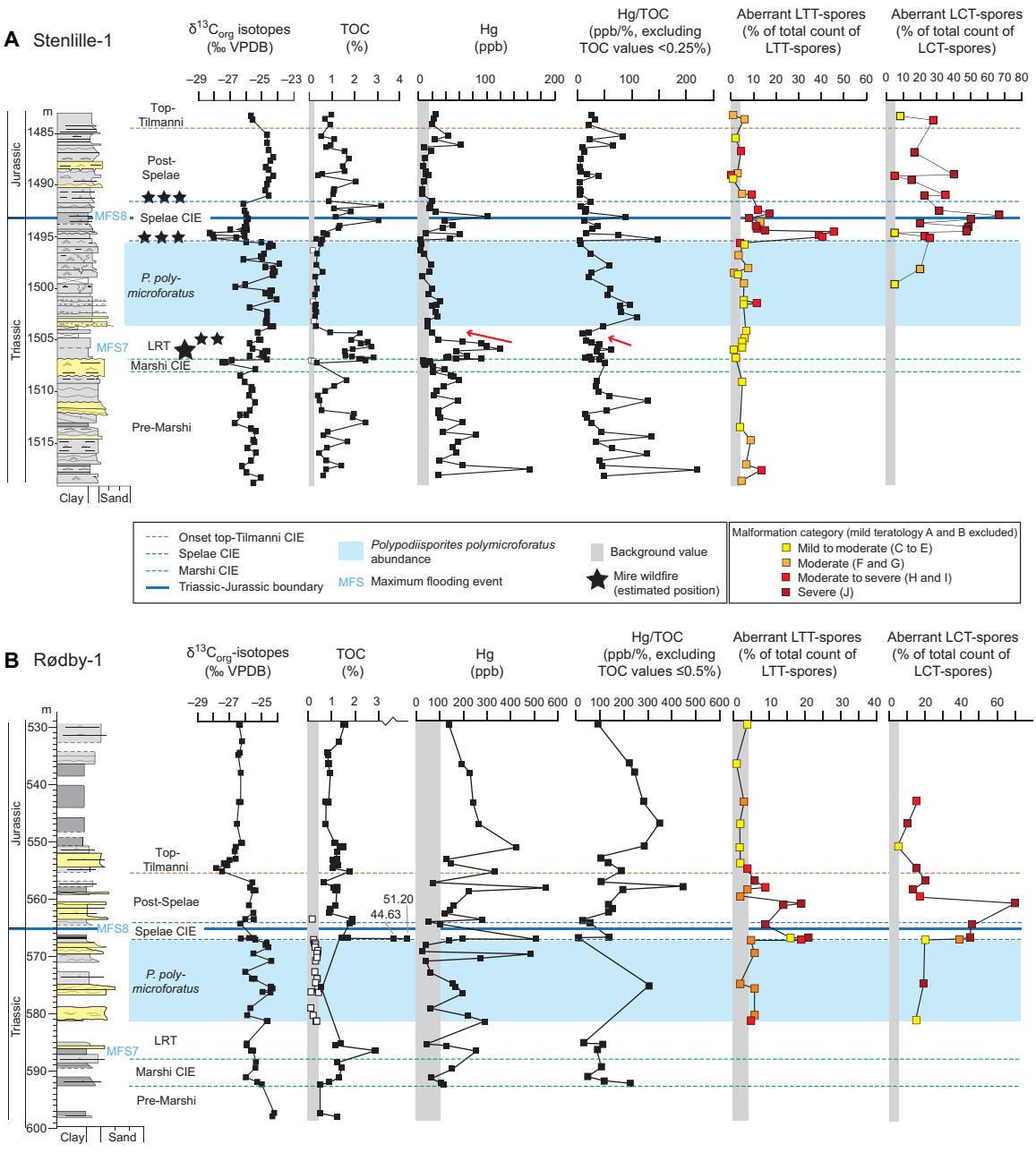

Fig. 3. Organic $\delta^{13}C$, total organic carbon, Hg loading and Hg/TOC, and total teratology for Stenlille-1 and Rødby-1. (**A**) Stenlille-1, and (**B**) Rødby-1. The LTT- and LCT-spore teratology is expressed as percentage of the total number of specimens counted within each genus per sample, as well as total severity of sample expressed as colors. Lithology and intervals used to subdivide the TJB succession mainly after reference (*32*). Stars denote approximate position of terrestrial coal/coaly beds in the Danish Basin (*45*). Number of stars indicates frequency of wildfires. Larger star size indicates higher estimated burning temperature (*45*). Red arrows on (A) mark levels where Hg and Hg/TOC decrease, while TOC levels remain high. Note that TOC values below the detection levels are marked with white squares and that no Hg/TOC values were calculated for these samples. VPDB, Vienna Pee Dee belemnite.

[severity categories (C) and (E) to (H); Figs. 3 and 4; and fig. S3], i.e., primarily indicating aborted spores and mild deformation of labra, but with a few specimens indicating disturbed meiosis, unbalanced and incomplete cytokinesis (cell division), and occasional deformation of proximal germination area (Table 1). During the upper pre-Marshi, Marshi, and lower LRT intervals, malformations are restricted to minor to moderate mutagenesis [severity categories (C) to (E), Table 1] and, apart from at one level in the terrestrial site where aberrant specimens comprise 20% of the counted LTT-spores, aberrant spores never exceed 8% (Figs. 3 and 4 and tables S2 to S5). From the upper part of the LRT and through the *P. polymicroforatus* interval, malformed LTT-spores with increased mutagenic severity occur more consistently (Figs. 3 and 4). A similar trend is also noted in the terrestrial site that only covers a minor part of the interval (Figs. 3 and 4 and fig. S4). The mutagenic teratology in LTT-spores culminates during and just after the Spelae CIE in all three cores, with abundant occurrences in all teratological categories including moderate to severe and severe teratology [severity categories (H) to (J), Table 1 and fig. S3). At this

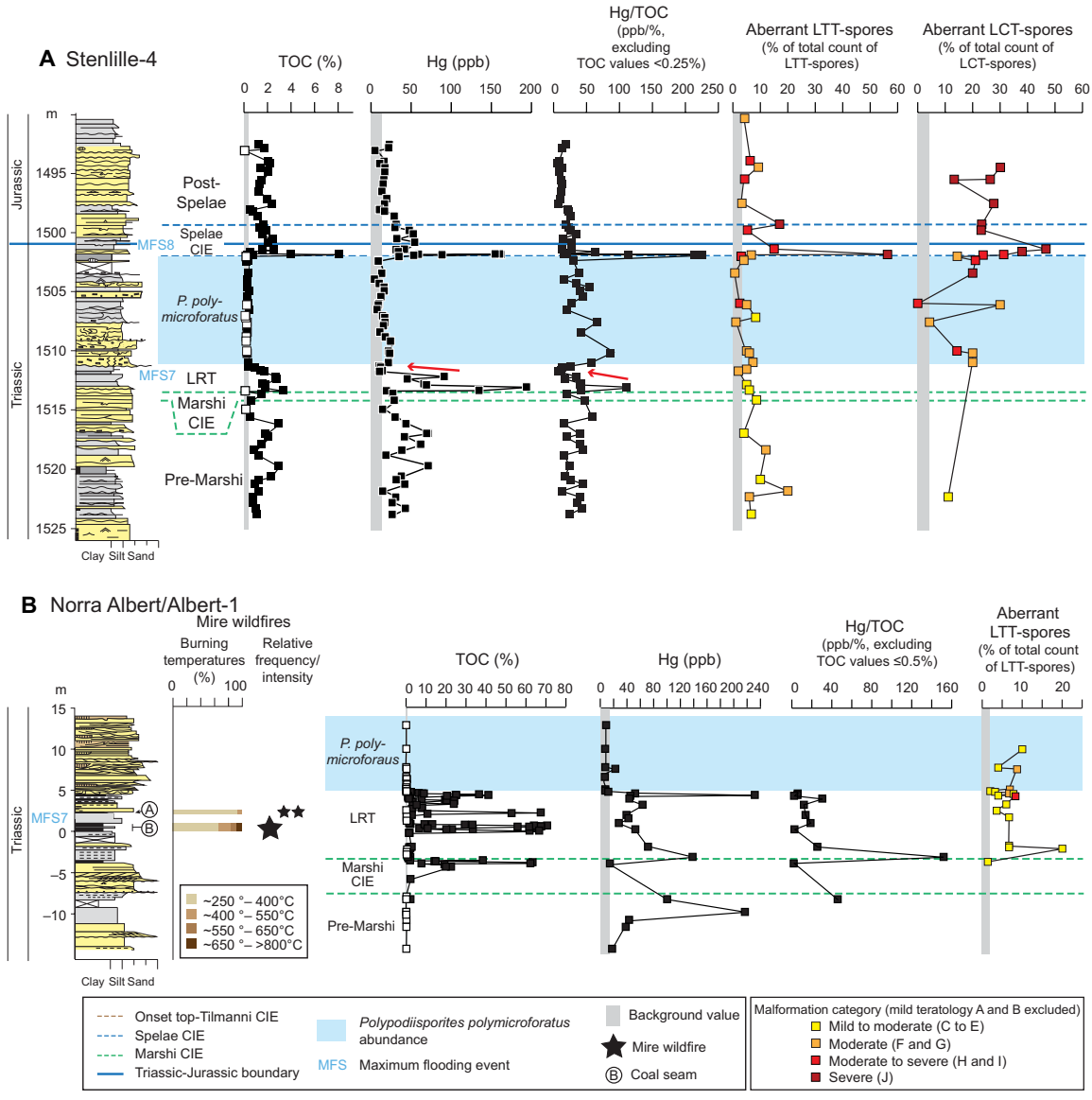

Fig. 4. TOC, Hg loading and Hg/TOC, and total teratology for Stenlille-4 and Norra Albert/Albert-1. (**A**) Stenlille-4 and (**B**) Norra Albert/Albert-1. The LTT- and LCT-spore teratology is expressed as percentage of the total number of specimens counted within each genus per sample, as well as total severity of sample expressed as colors. Lithology and intervals used to subdivide the TJB succession mainly after (*36*). Red arrows on (A) mark levels where Hg and Hg/TOC decrease, while TOC levels remain high. Note that TOC values below the detection levels are marked with white squares and that no Hg/TOC values were generated for these samples.

level, aberrant forms can encompass as much as 56% of the counted LTT-spores (Stenlille-1, 11 to 45%; Stenlille-4, 12 to 56%; Rødby-1, 9 to 21%) (Figs. 3 and 4, fig. S3, and tables S2 to S4). During the post-Spelae interval, mutagenic LTT-spores are encountered less frequently, commonly not constituting more than 5% of the counted LTT-spores. There is a slight increase of up to 9% around the top-Tilmanni CIE, with occasionally more severe teratology (Figs. 3 and 4, fig. S3 and tables S2 to S4).

LCT-spores are present but generally rare in the pre-Marshi, Marshi, and LRT intervals, and therefore, no quantitative assessments of the teratology of these spores could be carried out at these levels. LCT-spores first become more abundant during the *P. polymicroforatus* interval. However, LCT-spores are generally less abundant than the LTT-spores. The abundance curve for aberrant LCT-spores is similar to that of the LTT-spores, especially in Rødby-1, with the highest abundances and severities recorded during and after the Spelae CIE (Figs. 3 and 4 and tables S6 to S8). The percentage of aberrant forms is exceptionally high in some samples, often exceeding 40% of the counted LCT-spores (67% at one level in Stenlille-1 and 70% at one level in Rødby-1). These samples contain abundant specimens assigned to severity category (J), where the entire proximal face of the spore is deformed to the extent that the proximal mark can no longer be recognized (Fig. 2II). Circular forms with this type of deformation has routinely been counted as aberrant LCT-spores, while more triangular forms with similar deformation have been assigned to aberrant LTT-spores (compare Fig. 2II with fig. S1P). However, there is a possibility that some of these forms include aberrant polyploid LTT-spores, as polyploid specimens in some extant ferns that normally produce triangular spores have been noted to be larger and more rounded in shape [see, e.g., (*26*)].

DISCUSSION

The narrow, well-defined levels with high concentrations of Hg in the studied successions can be correlated between the sites within the Danish and North German basins and suggest that Hg deposition was pulsed (Figs. 3 and 4 and fig. S4). Using the stratigraphic framework (*32*) described above, we correlate our new Hg/TOC record for Stenlille-1 with the previously published Hg/TOC records from the New York Canyon (*16*) and Kuhjoch (*17*) (Fig. 1 and fig. S2). Despite major differences in sedimentation rates, as well as amplitudes in the organic CIEs between all localities, both the Hg/TOC records and the $\delta^{13}C$ records are fairly consistent (Fig. 1 and fig. S2). This bio- and chemostratigraphic correlation between the sedimentary successions and CAMP rocks indicate a temporal link between Hg loading and volcanic activity (Fig. 1). The CIEs have been attributed to CO_2 or methane emissions from CAMP volcanism (*4*, *5*) and more recently from magma-sediment interaction (*40*). Because both the Hg loading (Hg and Hg/TOC) and the CIEs occur in discrete and repeated intervals (Fig. 1 and fig. S2), it is tempting to try to correlate individual Hg anomalies to specific CAMP eruptions. However, only two eruptive units of the CAMP have been dated by high-resolution U/Pb geochronology (the North Mountain and Preakness Basalts) (*1*, *7*, *8*). These two eruptive units are separated by an interval, with minimum duration of 164 ka according to the U/Pb ages (Fig. 1). The maximum age range for the ash beds constraining the marine mass extinction interval, as defined by ammonoids, encompasses the maximum phase of volcanic activity in the CAMP (Fig. 1 and fig. S2).

The Hg records of Stenlille-1 and Norra Albert/Albert-1 (Figs. 3 and 4) both extend further into the Rhaetian than the records from Kuhjoch and Nevada (Fig. 1), and both indicate a pre-Marshi perturbation to the Hg cycle. This perturbation may therefore be related to older CAMP eruptions. These older eruptions have been indicated by mineralogical and geochemical signatures of Triassic sediments below the oldest CAMP basalt in Morocco (*41*). Both the LRT interval and the Spelae CIE are associated with major Hg deposition in the Danish and North German basins, as well as in Nevada and Kuhjoch, suggesting widespread Hg perturbations at these levels (fig. S2). The Hg anomaly registered in the lower part of the LRT immediately succeeds the Marshi CIE. In the Kuhjoch record, this Hg anomaly occurs in highly condensed strata (*34*), which probably explains the high concentration of 555 ppb (*17*). Increased Hg is also registered just before the top-Tilmanni CIE [i.e., the main CIE of reference (*4*)] in all three records, but neither Hg/TOC records from Kuhjoch and Nevada show a convincing Hg anomaly at that level (Fig. 1 and fig. S2). In addition, an increase in Hg is also registered in the Rødby-1 record after the top-Tilmanni CIE (Fig. 3). This is in accordance with previous studies on Hg from LIP volcanism, where the Hg anomalies are not always matched by CIEs (*17*, *42*).

Marine and terrestrial Hg records can be expected to represent somewhat different but overlapping types of Hg deposition associated with massive volcanism. In the marine realm (based on the modern oceanic analog), atmospheric Hg was deposited mainly as oxidized Hg^{2+}, which was adsorbed and sedimented (i.e., scavenged) by marine algal organic matter (*43*). In the terrestrial environment, different processes would have prevailed. Oxidized Hg deposited onto soils would have been adsorbed by soil organic matter or taken up via roots by land plants, while freshwater algae may have absorbed Hg from the water. Terrestrial plants with stomata absorb substantial quantities of gaseous elemental Hg (Hg^0) directly from air, such that, in the modern world, the litterfall flux containing Hg^0 under all vegetation types is at least as important as oxidized Hg^{2+} deposition (*43*). Some terrestrial Hg ultimately finds its way to the ocean via rivers, but in the modern global budget, rivers contribute only about 10% of total ocean Hg inputs (*43*). Thus, if ancient oceans were like modern oceans, then the marine sedimentary successions represent mostly atmopsheric Hg deposited at the ocean surface.

The Hg/TOC ratio in sedimentary sequences is a reliable indicator for detecting substantial and sustained increases in atmospheric Hg deposition (*12*, *13*), particularly when interpreted in the context of Hg and TOC concentration data as we have done here. These increases in atmospheric Hg deposition lead to a sudden increase in Hg/TOC relative to the background in sediment records. On the basis of coincident changes in Hg and TOC concentrations, we interpret the elevated Hg/TOC as due to either a sudden rise in Hg concentration or a decrease in algal organic carbon production, both which result from the effects of massive volcanism (*12*, *13*). The relationship between Hg loading and Hg/TOC records in the investigated marine successions (Stenlille-1, Stenlille-4, and Rødby-1) indicates how the elevated Hg loading was drawn down by marine phytoplankton (Figs. 3 and 4). A recent study suggested that a high Hg/S ratio compared to a Hg/TOC ratio would demonstrate that Hg was bound to pyrite rather than organic matter in the marine sedimentary environment and that this would indicate a nonvolcanic source for Hg (*19*). This suggestion is in contradiction with the geochemistry of mercury in aqueous systems. Mercury is always associated with sulfur, as the dissolved bivalent Hg in the aquatic environment could potentially bind with either organosulfur compounds (thiols) or free sulfides, depending on their competitive binding kinetics (*12*, *44*). Therefore, Hg association with sulfur is not necessarily indicative of the source but rather of the complex geochemical conditions required for fixing dissolved Hg in the sediments (*12*, *44*). These considerations were thoroughly discussed in (*12*) (and references therein).

During the first part of the LRT, Hg is elevated in both the marine and terrestrial environments (Figs. 1, 3, and 4 and fig. S2). In the marine sections, high TOC levels result in low Hg/TOC levels during the first part of the LRT (Figs. 1, 3, and 4 and fig. S2). Elevated Hg/TOC values are only registered at one level within the lower part of the LRT in Stenlille-4. In the marine sections, the upper part of the LRT exhibits both decreasing Hg and Hg/TOC despite TOC levels remaining high (1 to 3%) (Figs. 3A and 4A levels marked with red arrows). We interpret this as indicating that the source of Hg was temporarily waning. In the terrestrial section, initially high Hg and Hg/TOC values in the first part of the LRT decrease upwards, while TOC remains constantly low (Fig. 4). Despite high TOC levels in the coals and coaly shales that contain plant remains accumulated over longer time intervals, Hg levels remain moderate and Hg/TOC levels are low, even in coal seams B and A that are known to contain charcoal (Fig. 4) (*45*). Hg/TOC only increases markedly in the uppermost coal sample, which despite high TOC indicates a temporary increase in input of Hg. After this, both TOC and Hg loading decrease markedly, partly as an effect of a major change in sedimentology (Fig. 4). The low TOC values during the *P. polymicroforatus* abundance interval could be a combination of increased sedimentation rates, decreased marine primary productivity (*9*), and deforestation on land (*36*). Despite the generally low TOC values throughout this interval, increased Hg/TOC levels are present in the lower part of the interval in all three cores (Figs. 3 to 5).

At the Spelae CIE, high Hg/TOC peaks correspond to increased Hg loading in all three marine records (Figs. 3 and 4), although increased

marine productivity increased at this level (*9*). During the post-Spelae interval, input of Hg to the basins was limited, indicating a period of quiescence in the volcanic activity. Slight increases in both Hg and Hg/TOC recorded just below the top-Tilmanni CIE in the Stenlille-1 and Rødby-1 records indicate renewed Hg supply to the basins (Figs. 3 and 4). This may continue above the top-Tilmanni CIE as indicated by increases in both Hg and Hg/TOC values at a higher stratigraphic level in Rødby-1 (Fig. 3).

The record of LTT-spore teratology across the TJB of the Danish and North German basins, varies in concert with the volcanic activity, as inferred by the C-isotope and Hg records (Figs. 3 to 5). The marked abundance of malformed LTT- and LCT-spores has also been noted at the equivalent stratigraphic levels in localities in southern Sweden (Supplementary Text), Germany (*41*), and at the Global Stratotype Sections and Point locality Kuhjoch in Austria (*41*), indicating supra-regional environmental conditions stressing land plants at this time. During the TJB, LTT-spores were produced primarily by the fern families Dipteridaceae, Dicksoniaceae, and Matoniaceae, while LCT-spores were primarily produced by ferns belonging to Osmundaceae and Marattiales (*46*).

Many fern families have naturally occurring apogamy, which can involve as much as 17% of the local flora (*47*). Apogamy is an asexual reproductive process in which a new sporophyte is developed directly from the gametophyte without fusion of gametes, and this process can result in the production of high percentages of malformed spores in subsequent generations due to the resulting polyploidy of the hybrid plant. However, among ferns, apogamy with or without polyploidy is restricted to certain families (*47*). The known parent fern families of the herein recorded Triassic-Jurassic spores, namely, the Dipteridaceae, the Matoniaceae, and the Dicksoniaceae (and possibly also including the Cyathaceae, the Cibotiaceae and the Gleicheniaceae) for the LTT-spores, and the Osmundaceae and the Marattiaceae for the LCT-spores, do not exhibit apogamy (*47*). This fact makes the mass occurrence of aberrant spores among these families at the TJB even more remarkable.

The teratology across the TJB also indicates a pulsed nature of the mutagenesis, with increased abundances and severity in malformations over the extinction interval and culminating during the Spelae CIE (Fig. 5). This pulsed temporal correlation between the Hg loading and the teratology suggests a causal link between the mutagenesis and the volcanism (Fig. 5).

For recorded spore and pollen mutagenesis during the end-Permian event, a scenario involving ozone layer depletion due to emissions of halocarbons and aerosols from the Siberian Traps LIP was proposed (*27*). During that event, malformed bisaccate pollen registered in Permian-Triassic boundary strata reached abundances of up to 6% (*24*). This is a plausible scenario also for the end-Triassic event due to a magma-evaporite interaction caused by intrusion of Brazilian low-titanium sills (*40*), although in our TJB successions, aberrant pinacean and other bisaccate gymnosperm pollen have only been noted in very low numbers, much lower than at the Permian-Triassic boundary. It therefore seems likely that the high abundances of LTT- and LCT-spores at the TJB were caused by a mechanism other than increased UV-B radiation.

The TJB, and specifically the Spelae CIE, is associated with marked global warming, recorded by stomatal proxy data, and estimated to have increased mean global temperatures by 2.5° to 5°C (*48*). An experimental study involving high localized temperature treatment (38° to 40°C) of extant angiosperm pollen shows polyploidy, abnormal meiosis, and cytokinesis during pollen formation (*49*). However, there is a marked difference between localized heating of pollen producing organs to 38° to 40°C and prolonged ambient air temperature of the same magnitude. These high air temperatures during an extended period of time would most likely repress most of the vegetation, and few plants could survive long-term temperatures above 40°C (*50*). In addition, during the Spelae CIE, the terrestrial ecosystem appears to be recovering, with the return of gymnosperm vegetation (*9*). Thus, although neither ozone layer depletion nor global warming can be ruled out as contributing causes of the malformed fern spores at the TJB, they most likely were not the main cause. One group of phytotoxic substances that have been recorded in TJB successions in Germany, Poland, and Greenland are PAHs (*36*, *51*, *52*), which have been suggested to have formed either by thermal reactions between CAMP-intrusive magma and organic rich sediments or from wildfires. However, in the Mariental core in the North German Basin, where aberrant LTT-spores and increased PAHs are recorded within the same interval, the aberrant LTT-spores decreased in abundance, while PAHs continued to be registered upsection (*35*, *36*). This discrepancy suggests that PAHs were not the main mutagenic trigger.

On the basis of our results, we instead propose that the observed teratology is an expression of Hg toxicity in the parent plants. As one of the most toxic elements on the planet, mercury can cause both visible injuries and physiological disorders in plants (*53*), including stomatal closure, disturbed mitochondrial activity, and induced oxidative stress, which, in turn, damage DNA (*21*, *54*–*55*). Today, mercury pollution from anthropogenic sources is known to seriously disturb growth and reproductive cycles in plants, causing long-term effects on soil fertility and subsequent severe health issues to animals and human population (*21*, *54*, *55*). This is because mercury, primarily as methylmercury, bioaccumulates and biomagnifies via the food chain (*54*). Recent studies on Hg toxicity in plants show that mercury causes similar interference in plant cells as other heavy metals (*55*), causing DNA damage through reactive oxygen species formation, interacting with proteins used for replication or repair of DNA, or by binding directly to negative centers (e.g., phosphorous) in the DNA and causing mutagenesis (*55*). If DNA repair mechanisms become dysfunctional, then damages to DNA will be transferred to the next generation; i.e., Hg-induced mutagenic changes on plant DNA can be transferred to the reproductive cells, in this case spores. Although the parent ferns of LTT- and LCT-spores produced excessive amounts of malformed spores at the TJB, these plants persisted and continued to be an important part of mid-Mesozoic terrestrial ecosystems. In contrast, many of the typical Late Triassic plants that went extinct during the end-Triassic event, as shown by macroplant and palynological records (*37*, *38*), may have had less opportunistic growth and reproductive strategies and lower tolerance to phytotoxicity than the resilient parent ferns of LTT- and LCT-spores.

The coastal Rhaetian forest mires of the Danish and North German basins, as well as the forests in Greenland (*45*, *56*), were areas that also acted as catchments and may both have received and stored high amounts of Hg from CAMP (*57*). It is possible that increased wildfire intensity across the TJB could have further exacerbated the phytotoxic effects of direct Hg deposition by redistributing Hg from CAMP previously stored in plants, peats, and soils (*45*, *56*, *57*). However, note that the mire wildfire records of the Danish Basin (*45*) do not seem to coincide with the Hg or Hg/TOC anomalies in our records (Figs. 3 and 4). Similarly, it is not obvious from the charcoal (*56*), Hg, and Hg/TOC records (*17*) across the terrestrial

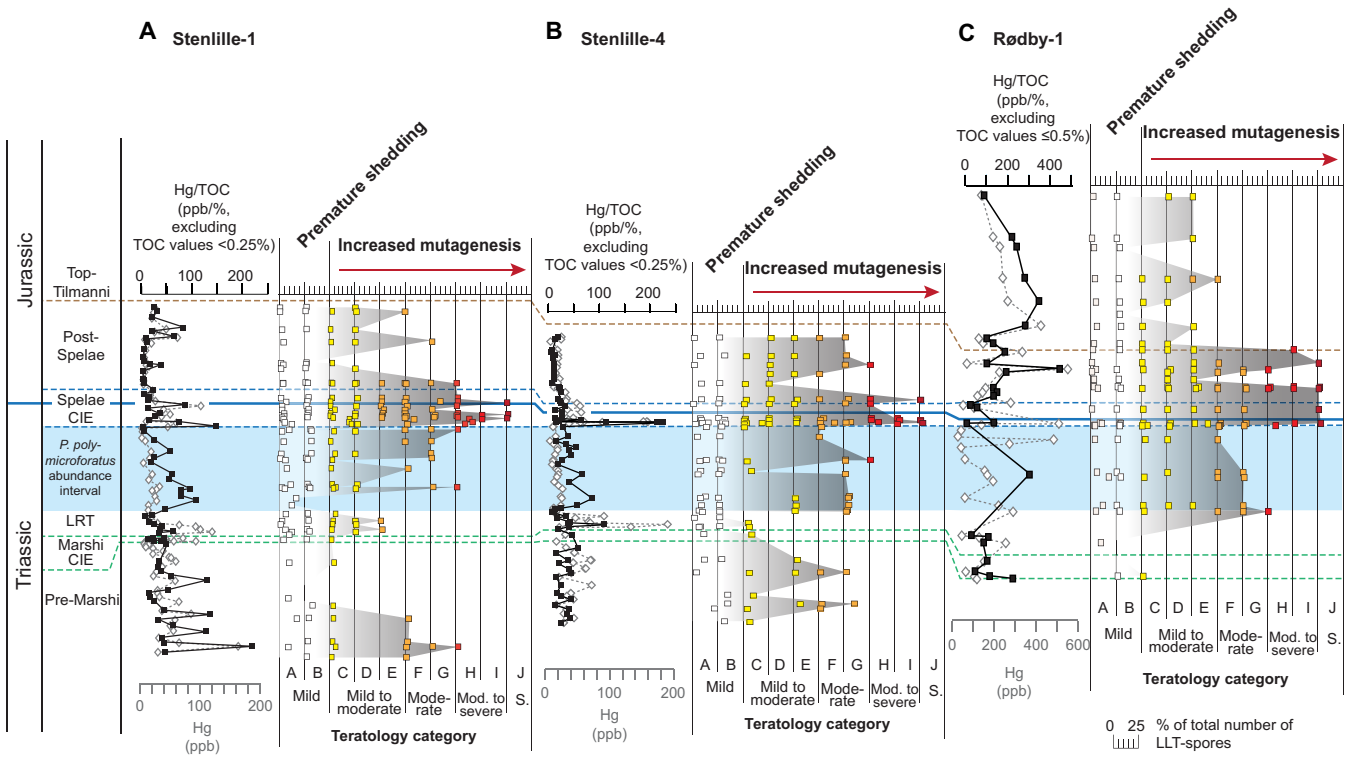

Fig. 5. Hg loading and Hg/TOC versus cumulative abundance and severity of LTT-spore teratology. (**A**) Stenlille-1, (**B**) Stenlille-4, and (**C**) Rødby-1. (A) to (J) Teratological severity categories; characteristics can be found in Table 1. Original plots for the cumulative abundance and severity can be found in fig. S2 to S4, and the data are listed in tables S2 to S4.

TJB in Greenland that the Hg anomalies were linked to wildfires (fig. S5).

Our combined mercury and teratology records demonstrate that terrestrial plants in NW Europe were subject to mutagenesis correlative with CAMP volcanism. Thus, in addition to environmental stress from global warming (*48*) and sulfuric acid deposition (*58*) due to emissions from CAMP, mercury-induced phytotoxicity may have played a role in the demise of Late Triassic land plants. However, future work should focus on assessing the teratology of various groups of fossil spores and pollen across LIP-linked extinctions to unravel the exact cause or causes of the mutagenesis. The close correlation, between the teratology across the TJB and the intensity of CAMP volcanic activity, emphasizes that environmental stress due to prolonged degassing of greenhouse gases and toxic compounds from LIPs could be an important factor in past floral extinctions.

MATERIALS AND METHODS

Experimental design

During routine quantitative analysis, aberrant palynomorphs were found to be exceptionally abundant over the TJB interval in the Danish and North German basins. In normal sporogenesis, the spore/pollen mother cell (2*n*), through double meiosis, forms a spore/pollen tetrad in which each spore/pollen is haploid (*n*). This normally results in 96% viable spores or pollen and a minor number, <4%, aberrant and nonviable spores or pollen (*26*). This is in accordance with studies on both fossil and extant bisaccate pollen from sporangia, which contained 3 to 5% abnormal grains (*24*–*26*). As an example, of the 4.5% aberrant pollen in Permian glossopterid sporangia from Antarctica, 4% were not fully expanded grains, and 0.5% pollen exhibited mutagenic changes, i.e., had either only one saccus or extra sacci (*25*). Increased amounts of aberrant spores and pollen can form in several ways. Nonmutagenic changes can be induced through environmental stresses (e.g., drought, frost, and water logging) by disrupting the meiotic process during spore or pollen formation. In many cases, the environmental stress is seasonal and may only affect parts of a population and will often only result in increased amounts of immature, i.e., prematurely shed, spores or pollen that may or may not still be retained in tetrads when found dispersed. A disturbed meiotic process can sometimes lead to production of natural polyploids, i.e., viable diploid (2*n*) spores or pollen morphologically identical to normal haploid spores, except for a marked increase in size. This process is often an evolutionary advantage, as polyploid plants tend to be more vigorous and better at colonizing disturbed habitats (*26*). In present-day environmental studies, increased abundances of aberrant spores and pollen have been used as indicators of radioactivity (*59*), industrial pollution (*23*), and heavy-metal toxicity (*22*). To assess whether the increased abundance of aberrant spores and pollen were linked to emissions from the CAMP volcanism, this study was designed to combine records of teratology and Hg loading.

Mercury

Total bulk analysis of Hg was conducted using a Milestone DMA-80 direct Hg analyzer, following the ASTM D6722-01 standard method (American Society for Testing and Materials, 2006) in the Geological Survey of Canada. Mercury was also analyzed using a LECO AMA254 mercury analyzer at the University of California, Davis by the same procedure. Gaseous elemental Hg was vaporized from the samples

after heating at 800°C and then collected on a gold amalgamation trap for subsequent quantification using atomic absorption spectrometry. The standard reference materials used for this study included the National Institute of Standards and Technology (NIST) 2683B Coal with a certified value of 0.094 ± 0.004 μg/g Hg [laboratory quality control (QC) data, 0.091 ± 0.004 μg/g Hg] and NIST 1633B Fly Ash with a certified value of 0.141 ± 0.019 μg/g Hg (QC data, 0.141 μg/g ± 0.005 μg/g Hg). Duplicate analyses were carried out on nine samples from Stenlille-4 with Hg values ranging from 9.8 to 160.3 ppb with a mean analytical error of ±0.01%. All mercury data are listed in table S9.

Total organic carbon

For samples from Stenlille-1 and Stenlille-4, the TOC [weight % (wt %)] was measured on approximately 50 mg of bulk dry samples using Rock-EVal 6 analysis at the Geological Survey of Canada with a detection limit for TOC of 0.24%. No TOC values below the detection limit were used for assessing Hg/TOC. For Rødby-1 and Norra Albert/Albert-1, sample powders were first treated with 10% HCl to dissolve any carbonates and centrifuged followed by decanting the supernatant. The remnants were washed with ultrapure Milli-Q water five to six times sufficient to neutralize the supernatant. Slurries were then dried for 36 to 48 hours at 50°C, reground in an agate mortar, and returned to the drying oven for several hours at 110°C. Powder (250 to 500 mg) was loaded in ceramic crucibles, and total (organic) carbon was analyzed with an Elementar Vario MAX CNS analyzer using the "Soil40" method in the Department of Geoscience, Aarhus University. Blanks, the sulfadiazine calibration standard, and working standard [Aarhus University (AU) 780523] were run at the beginning and end of each session and after every 10 samples. Blanks were <0.035 wt % C, while the AU standard was reproducible within 0.3% at 1.94 wt % C. For Rødby-1 and Norra Albert/Albert-1, no TOC values below 0.5% were used for assessing Hg/TOC. All TOC data are listed in table S9.

Palynology

The samples were prepared at the Geological Survey of Denmark and Greenland using standard palynological methods involving digestion of 20 g of sediment in hydrochloric and hydrofluoric acid, mild oxidation, and filtering of the organic residues over 11-μm mesh filter (*60*). Two to three strew slides were mounted per sample, using glycerine gel. To assess the percentage of aberrant forms, all normal and aberrant specimens of LTT- and LCT-spores were counted separately within one strew slide from each sample (tables S2 to S5), using a Leica DM 2000 transmitted light microscope fitted with a differential interference contrast system. During counting, the strew slides were scanned systematically using a ×40 lens (506097, Leica) along transverse transects, until the entire slide was scanned or until ≥100 specimens were counted. Only specimens that exhibit clear signs of aberrancy were counted as aberrant. Because folded, broken, or obscured specimens were always counted as normal, the obtained aberrancy values may be an underestimation. In some samples, statistical significance could not be obtained, and the results were disregarded in the plots in Figs. 3 to 5 and figs. S2 and S4. LCT-spores were generally much less abundant than the LTT-spores. The quantitative data are presented in tables S2 to S7.

Teratology

To assess the teratology, we focused on the aberrant spore data for two morphological groups that have relatively simple morphologies and sufficient exine thickness to enable distinction between true malformations and preservational artifacts. The first morphogroup, LTT-spores, comprises laevigate, triangular, trilete spores, which, during the Rhaetian and Early Jurassic in NW Europe, are known to have been produced by ferns of the Dipteridaceae, Dicksoniaceae, or Matoniaceae (*46*). The second morphogroup, the LCT-spores, comprises laevigate, circular, trilete spores that are known to have been produced by ferns assigned to the Osmundaceae or Marattiales (*46*). Thus, these two morphogroups are both most likely derived from heterogeneous mother plants that may have had different ecological preferences. The LTT-morphogroup includes spores that could, if found dispersed, be assigned to several different form taxa, including *Cyathidites*, *Concavisporites*, *Deltoidospora*, and *Dictyophyllidites*. This also includes some form taxa that are herein regarded as aberrant forms but that have been described as species of their own in published literature (Supplementary Text).

Rather than subdividing these fern spores according to form taxonomy on the species level, we focused on morphological traits related to function, i.e., viability (see below). The teratology may reflect different types of disturbance during spore formation, which may then indicate various forms of environmental stress. For this purpose, the teratologies were categorized on a five-step severity scale during the counts (Table 1 and fig. S3). In some cases, spores exhibited several types of teratogeny, in which case they were classified after the severest form. Each sample was categorized according to the maximum severity of the teratology in that sample.

Mild teratology

Usually, dwarfed forms could be distinguished from normal spores by their denser exine and underdeveloped character, but occasionally, the spores were merely unusually small in size. In the latter case, the spores may still have been viable. Dwarfed forms and unexpanded forms were considered to represent mild teratology and were primarily considered to have formed because of premature shedding from the sporangia (Fig. 2, G to K). Unexpanded forms were most likely nonviable, as they never matured.

Mild to moderate teratology

Uneven trilete rays, aberrant folding or cracking of the exine, and thickened labra or labra with deformations (i.e., growths, commonly in the form of verrucae or baculae) were considered mild to moderate teratology (Table 1 and Fig. 2, H to V). Uneven trilete rays may have developed if one or more of the spores in a spore tetrad had not matured when the spores are shed (Fig. 2, L to N, and fig. S1, F and G). Spores with thickened labra, exemplified by Fig. 2 (T and U) have previously been described as a separate for taxon (Supplementary Text) but were herein considered malformed. Aberrant folding and cracking of the exine are enigmatic features, which may indicate genetic disturbance that affected the concentration of sporopollenin in the spore wall (Fig. 2, N to P, V, DD, and II, and fig. S1O). Specimens similar to these were often assigned to specific form taxa in the literature (Supplementary Text). Cracking of the exine was often also associated with more severe teratology. They were placed here within the mild to moderate teratology category, as these features may not necessarily have rendered the spores nonviable. Similarly, abnormally wide labra or labra with growths were also considered to have formed because of a minor genetic disturbance, but since the outline and size of the spores often appeared normal, the spores may still have been viable.

Moderate teratology

Mono- or multilete marks and deformed outline were classified as moderate aberrancies (Fig. 2, W to CC). Spores with monolete marks

instead of trilete marks were either formed in a tetragonal instead of a tetrahedral tetrad or by unbalanced cytokinesis (Fig. 2, X to AA, and fig. S1K). A multilete mark also demonstrated malfunctioning meiosis where the spore mother cell was divided into more than four spores (Fig. 2, W, EE, and HH). A deformed outline was usually expressed as an invagination of the spore wall. In LTT-spores, this invagination was often located near one of the radial apices (Fig. 2, AA to DD and FF). This invagination could possibly be a remnant of malfunctioning or incomplete cytokinesis.

Moderate to severe teratology

This included weakly deformed proximal area (i.e., laesura still discernable) and deformed tetrads (including fused tetrads) (Fig. 2, DD to GG). The weakly deformed proximal area was expressed as thickening and wrinkling of the proximal area, which often partially affected or distorted the trilete mark (Fig. 2, DD to FF, and fig. S1, L and M). Deformed tetrads included fused tetrads, tetrads with various sized spores, and also fused dyads (Fig. 2GG and fig. S1N) and was characterized by at least one of the individual spores being morphologically deformed. Both these teratologies were interpreted as reflecting genetic disturbance resulting in nonviable spores.

Severe teratology

This included only spores with severely deformed proximal areas, where the laesurae were no longer discernable (Fig. 2, HH and II, and fig. S1, O and P). These spores were nonviable.

SUPPLEMENTARY MATERIALS

Supplementary material for this article is available at http://advances.sciencemag.org/cgi/content/full/5/10/eaaw4018/DC1

Supplementary Text

Fig. S1. Selected photographs of LTT-spores teratology, arranged after teratology categories defined in Table 1.

Fig. S2. Expanded correlation from Fig. 1.

Fig. S3. Plots showing the stratigraphic occurrence and abundance of each teratological form of LTT-spores.

Fig. S4. Correlation between the localities studied herein.

Fig. S5. Correlation of organic C-isotopes (*4*), charcoal data (*56*), PAH (*52*), and mercury data (*17*) from Astartekløft, Greenland.

Table S1. Sample and slide numbers and England Finder coordinates for the LTT-spores illustrated in Fig. 2.

Table S2. Stenlille-1: Counts of total and aberrant LTT-spores.

Table S3. Stenlille-4: Counts of total and aberrant LTT-spores.

Table S4. Rødby-1: Counts of total and aberrant LTT-spores.

Table S5. Norra Albert/Albert-1: Counts of total and aberrant LTT-spores.

Table S6. Stenlille-1: Counts of total and aberrant LCT-spores.

Table S7. Stenlille-4: Counts of total and aberrant LCT-spores.

Table S8. Rødby-1: Counts of total and aberrant LCT-spores.

Table S9. Mercury and TOC values for the investigated localities.

Table S10. Sample and slide numbers and England Finder coordinates for the LCT-spores illustrated in fig. S1.

References (*61*–*76*)

REFERENCES AND NOTES

1. B. Schoene, J. Guex, A. Bartolini, U. Schaltegger, T. J. Blackburn, Correlating the end-Triassic mass extinction and flood basalt volcanism at the 100 ka level. *Geology* **38**, 387–390 (2010).
2. J.-F. Wotzlaw, J. Guex, A. Bartolini, Y. Gallet, L. Krystyn, C. A. McRoberts, D. Taylor, B. Schoene, U. Schaltegger, Towards accurate numerical calibration of the Late Triassic: High-precision U-Pb geochronology constraints on the duration of the Rhaetian. *Geology* **42**, 571–574 (2014).
3. G. R. McGhee Jr., M. E. Clapham, P. M. Sheehan, D. J. Bottjer, M. L. Droser, A new ecological-severity ranking of major Phanerozoic biodiversity crises. *Palaeogeogr. Palaeoclimatol. Palaeoecol.* **370**, 260–270 (2013).
4. S. P. Hesselbo, S. A. Robinson, F. Surlyk, S. Piasecki, Terrestrial and marine extinction at the Triassic-Jurassic boundary synchronized with major carbon-cycle perturbation: A link to initiation of massive volcanism? *Geology* **30**, 251–254 (2002).
5. M. Ruhl, N. R. Bonis, G.-J. Reichart, J. S. Sinninghe Damsté, W. M. Kürschner, Atmospheric carbon injection linked to end-Triassic mass extinction. *Science* **333**, 430–434 (2011).
6. A. Marzoli, S. Callegaro, J. Dal Corso, J. H. F. L. Davies, M. Chiaradia, N. Youbi, H. Bertrand, L. Reisberg, R. Merle, F. Jourdan, The Central Atlantic Magmatic Province: A review, in *The Late Triassic World*, L. H. Tanner, ed. (Topics in Geobiology 46, Springer, 2018), chap. 4.
7. J. H. F. L. Davies, A. Marzoli, H. Bertrand, N. Youbi, M. Ernesto, U. Schaltegger, End-Triassic mass extinction started by intrusive CAMP activity. *Nat. Commun.* **8**, 15596 (2017).
8. T. J. Blackburn, P. E. Olsen, S. A. Bowring, N. M. McLean, D. V. Kent, J. Puffer, G. McHone, E. T. Rasbury, M. Et-Touhami, Zircon U-Pb geochronology links the end-triassic extinction with the Central Atlantic Magmatic Province. *Science* **340**, 941–945 (2013).
9. S. Lindström, B. van de Schootbrugge, K. Dybkjær, G. K. Pedersen, J. Fiebig, L. H. Nielsen, S. Richoz, No causal link between terrestrial ecosystem change and methane release during the end-Triassic mass extinction. *Geology* **40**, 531–534 (2012).
10. J. Pálfy, N. Zajzon, Environmental changes across the Triassic-Jurassic boundary and coeval volcanism inferred from elemental geochemistry and mineralogy in the Kendlbachgraben section (Northern Calcareous Alps, Austria). *Earth Planet. Sci. Lett.* **335**, 121–134 (2012).
11. L. H. Tanner, F. T. Kyte, S. Richoz, L. Krystyn, Distribution of iridium and associated geochemistry across the Triassic-Jurassic boundary in sections at Kuhjoch and Kendlbach, Northern Calcareous Alps, Austria. *Palaeogeogr. Palaeoclimatol. Palaeoecol.* **449**, 13–26 (2016).
12. H. Sanei, S. E. Grasby, B. Beauchamp, Latest Permian mercury anomalies. *Geology* **40**, 63–66 (2012).
13. S. E. Grasby, H. Sanei, B. Beauchamp, Z. Chen, Mercury deposition through the Permo-Triassic Biotic Crisis. *Chem. Geol.* **351**, 209–216 (2013).
14. D. M. Pyle, T. A. Mather, The importance of volcanic emissions for the global atmospheric mercury cycle. *Atmos. Environ.* **37**, 5115–5124 (2003).
15. W. H. Schroeder, J. Munthe, Atmospheric mercury—An overview. *Atmos. Environ.* **32**, 809–822 (1998).
16. A. M. Thibodeau, K. Ritterbush, J. A. Yager, A. J. West, Y. Ibarra, D. J. Bottjer, W. M. Berelson, B. A. Bergquist, F. A. Corsetti, Mercury anomalies and the timing of biotic recovery following the end-Triassic mass extinction. *Nat. Commun.* **7**, 11147 (2016).
17. L. M. E. Percival, M. Ruhl, S. P. Hesselbo, H. C. Jenkyns, T. A. Mather, J. H. Whiteside, Mercury evidence for pulsed volcanism during the end-Triassic mass extinction. *Proc. Natl. Acad. Sci. U.S.A.* **114**, 7929–7934 (2017).
18. T. R. Them II, C. H. Jagoe, A. H. Caruthers, B. C. Gill, S. E. Grasby, D. R. Gröcke, R. Yin, J. D. Owens, Terrestrial sources as the primary delivery mechanism of mercury to the oceans across the Toarcian Oceanic Anoxic Event (Early Jurassic). *Earth Planet. Sci. Lett.* **507**, 62–72 (2019).
19. J. Shen, T. J. Algeo, J. Chen, N. J. Planavsky, Q. Feng, J. Yu, J. Liu, Mercury in marine Ordovician/Silurian boundary sections of South China is sulfide-hosted and non-volcanic in origin. *Earth Planet. Sci. Lett.* **511**, 130–140 (2019).
20. B. A. Bergquist, Mercury, volcanism, and mass extinctions. *Proc. Natl. Acad. Sci. U.S.A.* **114**, 8675–8677 (2017).
21. P. C. Nagajyoti, K. D. Lee, T. V. M. Sreekanth, Heavy metals, occurrence and toxicity for plants: A review. *Environ. Chem. Lett.* **8**, 199–216 (2010).
22. M. Gupta, S. Devi, Chronic toxicity of cadmium in *Pteris vittata*, a roadside fern. *Ecotoxicology* **3**, 235–247 (1994).
23. K. Mičieta, G. Murín, Microspore analysis for genotoxicity of a polluted environment. *Environ. Exp. Bot.* **36**, 21–27 (1996).
24. C. B. Foster, S. A. Afonin, Abnormal pollen grains: An outcome of deteriorating atmospheric conditions around the Permian - Triassic boundary. *J. Geol. Soc. London* **162**, 653–659 (2005).
25. S. Lindström, S. McLoughlin, A. N. Drinnan, Intraspecific variation of taeniate bisaccate pollen within Permian glossopterid sporangia, from the Prince Charles Mountains, Antarctica. *Int. J. Plant Sci.* **158**, 673–684 (1997).
26. E. W. Rabe, C. H. Haufler, Incipient polyploid speciation in the maidenhair fern (*Adiantum pedatum*, Adiantaceae)? *Am. J. Bot.* **79**, 701–707 (1992).
27. H. Visscher, C. V. Looy, M. E. Collinson, H. Brinkhuis, J. H. A. van Konijnenburg-van Cittert, W. M. Kürschner, M. A. Sephton, Environmental mutagenesis during the end-Permian ecological crisis. *Proc. Natl. Acad. Sci. U.S.A.* **101**, 12952–12956 (2004).
28. P. Filipiak, G. Racki, Proliferation of abnormal palynoflora during the end-Devonian biotic crisis. *Geol. Quart.* **54**, 1–14 (2010).
29. J. P. Benca, I. A. P. Duijnstee, C. V. Looy, UV-B-induced forest sterility: Implications of ozone shield failure in Earth's largest extinction. *Sci. Adv.* **4**, e1700618 (2018).
30. P. A. Hochuli, E. Schneebeli-Hermann, G. Mangerud, H. Bucher, Evidence for atmospheric pollution across the Permian-Triassic transition. *Geology* **45**, 1123–1126 (2017).
31. B. van de Schootbrugge, P. B. Wignall, A tale of two extinctions: Converging end-Permian and end-Triassic scenarios. *Geol. Mag.* **153**, 332–354 (2016).

32. S. Lindström, B. van de Schootbrugge, K. H. Hansen, G. K. Pedersen, P. Alsen, N. Thibault, K. Dybkjær, C. J. Bjerrum, L. H. Nielsen, A new correlation of Triassic-Jurassic boundary successions in NW Europe, Nevada and Peru, and the Central Atlantic Magmatic Province: A time-line for the end-Triassic mass extinction. *Palaeogeogr. Palaeoclimatol. Palaeoecol.* **478**, 80–102 (2017).
33. T. H. Heimdal, H. H. Svensen, J. Ramezani, K. Iyer, E. Pereira, R. Rodrigues, M. T. Jones, S. Callegaro, Large-scale sill emplacement in Brazil as a trigger for the end-Triassic crisis. *Sci. Rep.* **8**, 141 (2018).
34. A. V. Hillebrandt, L. Krystyn, W. M. Kürschner, N. R. Bonis, M. Ruhl, S. Richoz, M. A. N. Schobben, M. Urlichs, P. R. Bown, K. Kment, C. A. McRoberts, M. Simms, A. Tomăsových, The Global Stratotype Sections and Point (GSSP) for the base of the Jurassic System at Kuhjoch (Karwendel Mountains, Northern Calcareous Alps, Tyrol, Austria). *Episodes* **36**, 162–198 (2013).
35. G. Barth, M. Franz, C. Heunisch, W. Ernst, J. Zimmermann, M. Wolfgramm, Marine and terrestrial sedimentation across the T-J transition in the North German Basin. *Palaeogeogr. Palaeoclimatol. Palaeoecol.* **489**, 74–94 (2018).
36. B. van de Schootbrugge, T. M. Quan, S. Lindström, W. Püttmann, C. Heunisch, J. Pross, J. Fiebig, R. Petschik, H. -G. Röhling, S. Richoz, Y. Rosenthal, P. G. Falkowski, Floral changes across the Triassic/Jurassic boundary linked to flood basalt volcanism. *Nat. Geosci.* **2**, 589–594 (2009).
37. S. Lindström, Palynofloral patterns of terrestrial ecosystem change during the end-Triassic event - a review. *Geol. Mag.* **153**, 223–251 (2016).
38. J. C. McElwain, M. E. Popa, S. P. Hesselbo, M. Haworth, F. Surlyk, Macroecological responses of terrestrial vegetation to climatic and atmospheric change across the Triassic/Jurassic boundary in East Greenland. *Paleobiology* **33**, 547–573 (2007).
39. G. Panfili, S. Cirilli, J. Dal Corso, H. Bertrand, F. Medina, N. Youbi, A. Marzoli, New biostratigraphic constraints show rapid emplacement of the Central Atlantic Magmatic Province (CAMP) during the end-Triassic mass extinction interval. *Global Planet. Change* **172**, 60–68 (2019).
40. T. H. Heimdal, S. Callegaro, H. H. Svensen, M. T. Jones, E. Pereira, S. Planke, Evidence for magma - evaporite interactions during the emplacement of the Central Atlantic Magmatic Province (CAMP) in Brazil. *Earth Planet. Sci. Lett.* **506**, 476–492 (2019).
41. J. Dal Corso, A. Marzoli, F. Tateo, H. C. Jenkyns, H. Bertrand, N. Youbi, A. Mahmoudi, E. Font, N. Buratti, S. Cirilli, The dawn of CAMP volcanism and its bearing on the end-Triassic carbon cycle disruption. *J. Geol. Soc. London* **171**, 153–164 (2014).
42. M. T. Jones, L. M. E. Percival, E. W. Stokke, J. Frieling, T. A. Mather, L. Riber, B. A. Schubert, B. Schultz, C. Tegner, S. Planke, H. H. Svensen, Mercury anomalies across the Palaeocene-Eocene Thermal Maximum. *Clim. Past* **15**, 217–236 (2019).
43. P. M. Outridge, R. P. Mason, F. Wang, S. Guerrero, L. E. Heimbürger-Boavida, Updated global and oceanic mercury budgets for the United Nations Global Mercury Assessment 2018. *Environ. Sci. Technol.* **52**, 11466–11477 (2018).
44. U. Skyllberg, A. Drott, Competition between disordered iron sulfide and natural organic matter associated thiols for mercury(II)–an EXAFS study. *Environ. Sci. Technol.* **44**, 1254–1259 (2010).
45. H. I. Petersen, S. Lindström, Synchronous wildfire activity rise and mire deforestation at the Triassic-Jurassic boundary. *PLOS ONE* **7**, e47236 (2012).
46. B. E. Balme, Fossil *in-situ* spores and pollen grains: An annotated catalog. *Rev. Palaeobot. Palynol.* **87**, 81–323 (1995).
47. H.-M. Liu, R. J. Dyer, Z.-Y. Guo, Z. Meng, J.-H. Li, H. Schneider, The evolutionary dynamics of apomixis in ferns: A case study from polystichoid ferns. *J. Bot.* **2012**, 510478 (2012).
48. M. Steinthorsdottir, A. J. Jeram, J. C. McElwain, Extremely elevated CO_2 concentrations at the Triassic/Jurassic boundary. *Palaeogeogr. Palaeoclimatol. Palaeoecol.* **308**, 418–432 (2011).
49. J. Wang, D. Li, F. Shang, X. Kang, High temperature-induced production of unreduced pollen and its cytological effects in *Populus*. *Sci. Rep.* **7**, 5281 (2017).
50. T. T. Kozlowski, S. G. Pallardy, Acclimation and adaptive responses of woody plants to environmental stresses. *Bot. Rev.* **68**, 270–334 (2002).
51. L. Marynowski, B. R. T. Simoneit, Widespread Upper Triassic to Lower Jurassic wildfire records from Poland: Evidence from charcoal and pyrolytic polycyclic aromatic hydrocarbons. *Palaios* **24**, 785–798 (2009).
52. K. H. Williford, K. Grice, A. Holman, J. C. McElwain, An organic record of terrestrial ecosystem collapse and recovery at the Triassic-Jurassic boundary in East Greenland. *Geochim. Cosmochim. Acta* **127**, 251–263 (2014).
53. Z. S. Zhou, S. Q. Huang, K. Guo, S. K. Mehta, P. C. Zhang, Z. M. Yang, Metabolic adaptations to mercury-induced oxidative stress in roots of *Medicago sativa* L. *J. Inorg. Biochem.* **101**, 1–9 (2007).
54. S. Malar, S. V. Sahi, P. J. C. Favas, P. Venkatachalam, Assessment of mercury heavy metal toxicity-induced physiochemical and molecular changes in *Sesbania grandiflora* L. *Int. J. Environ. Sci. Technol.* **12**, 3273–3282 (2015).
55. R. Azevedo, E. Rodriguez, R. J. Mendes, N. Mariz-Ponte, S. Sario, J. C. Lopes, J. M. P. F. de Oliveira, C. Santos, Inorganic Hg toxicity in plants: A comparison of different genotoxic parameters. *Plant Physiol. Biochem.* **125**, 247–254 (2018).
56. C. M. Belcher, L. Mander, G. Rein, F. X. Jervis, M. Haworth, S. P. Hesselbo, I. J. Glasspool, J. C. McElwain, Increased fire activity at the Triassic/Jurassic boundary in Greenland due to climate-driven floral change. *Nat. Geosci.* **3**, 426–429 (2010).
57. C. A. Eagles-Smith, J. G. Wiener, C. S. Eckley, J. J. Willacker, D. C. Evers, M. Marvin-DiPasquale, D. Obrist, J. A. Fleck, G. R. Aiken, J. M. Lepak, A. K. Jackson, J. P. Webster, A. R. Stewart, J. A. Davis, C. N. Alpers, J. T. Ackerman, Mercury in western North America: A synthesis of environmental contamination, fluxes, bioaccumulation, and risk to fish and wildlife. *Sci. Total Environ.* **568**, 1213–1226 (2016).
58. M. Steinthorsdottir, C. Elliott-Kingston, K. L. Bacon, Cuticle surfaces of fossil plants as a potential proxy for volcanic SO2 emissions: Observations from the Triassic-Jurassic transition of East Greenland. *Palaeobiodivers. Palaeoenviron.* **98**, 49–69 (2018).
59. O. F. Dzyuba, Teratomorphic pollen grains in modern and paleopalynological spectra and some problems of palynostratigraphy. *Neftegazovaya Geologiya: Teoriya I Praktika* **2**, (2007).
60. N. E. Poulsen, L. Gudmundsson, J. M. Hansen, Y. Husfeldt, *Palynological Preparation Techniques, A New Macerationtank-Method and Other Modifications*, Series C (Geological Survey of Denmark, 1990), vol. 10, pp. 1–23.
61. D. S. Jones, A. M. Martini, D. A. Fike, K. Kaiho, A volcanic trigger for the Late Ordovician mass extinction? Mercury data from south China and Laurentia. *Geology* **45**, 631–634 (2017).
62. G. Racki, M. Rakocinski, L. Marynowski, P. B. Wignall, Mercury enrichments and the Frasnian-Famennian biotic crisis: A volcanic trigger proved? *Geology* **46**, 543–546 (2018).
63. A. N. Sial, J. Chen, L. D. de Lacerda, R. Frei, V. C. Tewari, M. K. Pandit, C. Gaucher, V. P. Ferreira, S. Cirilli, S. Peralta, C. Korta, J. A. Barbosa, N. S. Pereira, Mercury enrichment and Hg isotopes in Cretaceous-Paleogene boundary successions: Links to volcanism and palaeoenvironmental impacts. *Cretaceous Res.* **66**, 60–81 (2016).
64. E. Font, T. Adatte, A. N. Sial, L. D. de Lacerda, G. Keller, J. Punekar, Mercury anomaly, Deccan volcanism, and the end-Cretaceous mass extinction. *Geology* **44**, 171–174 (2016).
65. A. Manceau, J. X. Wang, M. Rovezzi, P. Glatzel, X. B. Feng, Biogenesis of mercury-sulfur nanoparticles in plant leaves from atmospheric gaseous mercury. *Environ. Sci. Technol.* **52**, 3935–3948 (2018).
66. M. Patra, N. Bhowmik, B. Bandopadhyay, A. Sharma, Comparison of mercury, lead and arsenic with respect to genotoxic effects on plant systems and the development of genetic tolerance. *Environ. Exp. Bot.* **52**, 199–223 (2004).
67. H. Mosbæk, J. C. Tjell, T. Sevel, Plant uptake of airborne mercury in background areas. *Chemosphere* **17**, 1227–1236 (1988).
68. M. Wojciechowska-Mazurek, T. Zawadzka, K. Karlowski, K. Starska, K. Cwiek-Ludwicka, E. Brulinska-Ostrowska, Content of lead, cadmium, mercury, zinc and copper in fruit from various regions of Poland. *Rocz. Panstw. Zakl. Hig.* **46**, 223–238 (1995).
69. E. M. Suszcynsky, J. R. Shann, Phytotoxicity and accumulation of mercury in Tobacco subjected to different exposure routes. *Environ. Toxicol. Chem.* **14**, 61–67 (1995).
70. T. Sawidis, H.-D. Reiss, Effects of heavy metals on pollen tube growth and ultrastructure. *Protoplasma* **185**, 113–122 (1995).
71. K. K. Panda, M. Lenka, B. B. Panda, Monitoring and assessment of mercury pollution in the vicinity of a chloralkali plant. II Plant-availability, tissue-concentration and genotoxicity of mercury from agricultural soil contaminated with solid-waste assessed in Barley (*Hordeum vulgare* L.). *Environ. Pollut.* **76**, 33–42 (1992).
72. R. L. Petersen, P. C. Francis, Differential germination of fern and moss spores in response to mercuric chloride. *Am. Fern J.* **70**, 115–118 (1980).
73. J. J. Lund, Rhaetic to Lower Liassic palynology of the onshore southeastern North Sea Basin. *Danmarks Geologiske Undersøgelse II Raekke* **109**, 1–129 (1977).
74. W. Brenner, Bemerkungen zur Palynostratigraphie der Rhät-Lias-Grenze in SW-Deutschland. *Neues Jahrbuch im Geologie und Paläontologie (Abh.)* **173**, 131–166 (1986).
75. W. M. Kürschner, S. J. Batenburg, L. Mander, Aberrant *Classopollis* pollen reveals evidence for unreduced (2n) pollen in the conifer family Cheirolepidiaceae during the Triassic-Jurassic transition. *Proc. R. Soc. B Biol. Sci.* **280**, 20131708 (2013).
76. L. Mander, W. M. Kürschner, J. C. McElwain, Palynostratigraphy and vegetation history of the Triassic-Jurassic transition in East Greenland. *J. Geol. Soc. London* **170**, 37–46 (2013).

Acknowledgments: J. Halskov, Geological Survey of Denmark and Greenland (GEUS) helped with some of the illustrations. C.E.L. and C.T. also acknowledges support from the Danish National Research Foundation Niels Bohr Professorship for this research. **Funding:** This work was supported by the Geocenter Denmark grant 2013-6 (to S.L.) and benefitted from the grant ALW-OP.623 of the Dutch Science Foundation (NWO) (to B.v.d.S.). **Author contributions:** The project was designed by S.L. with input from H.S. and B.v.d.S. Palynological analyses were primarily carried out by S.L. with contributions from B.v.d.S., C.H., and K.D. The sedimentology was carried out by G.K.P. Mercury and TOC analyses were performed by H.S. and C.E.L., with input from C.T. The manuscript was developed by S.L., and all authors

contributed to editing the final manuscript. **Competing interests:** The authors declare that they have no competing interests. **Data and materials availability:** All data needed to evaluate the conclusions in the paper are present in the paper and/or the Supplementary Materials. Additional data related to this paper may be requested from the authors. All palynological slides are housed at the Geological Survey of Denmark and Greenland. Tables S1 and S10 list sample and slide numbers and England Finder coordinates for the photographed specimens. For quantitative teratological data, see tables S3 to S8. Mercury and TOC data are listed in table S9.

Submitted 17 December 2018
Accepted 13 September 2019
Published 23 October 2019
10.1126/sciadv.aaw4018

Citation: S. Lindström, H. Sanei, B. van de Schootbrugge, G. K. Pedersen, C. E. Lesher, C. Tegner, C. Heunisch, K. Dybkjær, P. M. Outridge, Volcanic mercury and mutagenesis in land plants during the end-Triassic mass extinction. *Sci. Adv.* **5**, eaaw4018 (2019).

ScienceAdvances

Volcanic mercury and mutagenesis in land plants during the end-Triassic mass extinction

Sofie Lindström, Hamed Sanei, Bas van de Schootbrugge, Gunver K. Pedersen, Charles E. Lesher, Christian Tegner, Carmen Heunisch, Karen Dybkjær and Peter M. Outridge

Sci Adv **5** (10), eaaw4018.
DOI: 10.1126/sciadv.aaw4018

Science Advances (ISSN 2375-2548) is published by the American Association for the Advancement of Science, 1200 New York Avenue NW, Washington, DC 20005. The title *Science Advances* is a registered trademark of AAAS.